Inorg. Chem. **2008**, *47*, 10308−10316

Spectroscopic Studies and Structures of *trans*-Ruthenium(II) and Ruthenium(III) Bis(cyanide) Complexes Supported by a Tetradentate Macrocyclic Tertiary Amine Ligand

Chun-Yuen Wong,[†,‡] Fu-Wa Lee,[†] Chi-Ming Che,*[,†] Yung Fong Cheng,[†] David Lee Phillips,[†] and Nianyong Zhu[†]

Department of Chemistry and HKU-CAS Joint Laboratory on New Materials, The University of Hong Kong, Pokfulam Road, Hong Kong SAR, China, and Department of Biology and Chemistry, City University of Hong Kong, Tat Chee Avenue, Kowloon, Hong Kong SAR, China

Received April 25, 2008

trans-[Ru(16-TMC)(C≡N)$_2$] (**1**; 16-TMC = 1,5,9,13-tetramethyl-1,5,9,13-tetraazacyclohexadecane) was prepared by the reaction of *trans*-[Ru(16-TMC)Cl$_2$]Cl with KCN in the presence of zinc powder. The oxidation of **1** with bromine gave *trans*-[Ru(16-TMC)(C≡N)$_2$]$^+$ isolated as PF_6 salt (**2**·PF_6). The Ru−C/C−N distances are 2.061(4)/1.130(5) and 2.069(5)/1.140(7) Å for **1** and **2**, respectively. Both complexes show a Ru(III/II) couple at 0.10 V versus $FeCp_2^{+/0}$. The UV−vis absorption spectrum of **1** is dominated by an intense high-energy absorption at λ_{max} = 230 nm, which is mainly originated from $d_\pi(Ru^{II}) \rightarrow \pi^*$(N≡C−Ru−C≡N) charge-transfer transition. Complex **2** shows intense absorption bands at $\lambda_{max} \leq 228$ nm and weaker vibronically structured absorption bands with peak maxima at 315−441 nm ($\varepsilon_{max} \approx (5-8) \times 10^2$ dm^3 mol^{-1} cm^{-1}), which are assigned to $d_\pi(Ru^{III}) \rightarrow \pi^*$(N≡C−Ru−C≡N) and $\sigma(^-C{\equiv}N) \rightarrow d(Ru^{III})$ charge-transfer transition, respectively. Density functional theory and time-dependent density-functional theory calculations have been performed on *trans*-[(NH$_3$)$_4$Ru(C≡N)$_2$] (**1′**) and *trans*-[(NH$_3$)$_4$Ru(C≡N)$_2$]$^+$ (**2′**) to examine the Ru−cyanide interaction and the nature of associated electronic transition(s). The 230 nm band of **1** has been probed by resonance Raman spectroscopy. Simulations of the absorption band and the resonance Raman intensities show that the nominal $\nu_{C\equiv N}$ stretch mode accounts for ca. 66% of the total vibrational reorganization energy. A change of nominal bond order for the cyanide ligand from 3 to 2.5 is estimated upon the electronic excitation.

Introduction

Transition metal complexes containing cyanide ligands have received considerable interest, as they are useful molecular building blocks for multinuclear oligomeric materials or solids with an extended structure.[1] Cyanide ion can act as a linear bridging ligand for two metal ions in a M$_1$−C≡N−M$_2$ manner. This bonding mode has been extensively used for the construction of 1-D chain, 2-D sheet, and 3-D giant networks, all of which possess interesting optical, electrical, and magnetic properties.[2] In this regard, transition metal hexacyanometalates [M(C≡N)$_6$]$^{n-}$ like Prussian blue (iron(III) hexacyanoferrate(II)) have been extensively studied as building blocks for the synthesis of functional materials with interesting

* Author to whom correspondence should be addressed. E-mail: cmche@hku.hk.
† The University of Hong Kong.
‡ City University of Hong Kong.

(1) (a) Fehlhammer, W. P.; Fritz, M. *Chem. Rev.* **1993**, *93*, 1243. (b) Hahn, F. E. *Angew. Chem., Int. Ed. Engl.* **1993**, *32*, 650.

(2) (a) Itaya, K.; Uchida, I.; Neff, V. D. *Acc. Chem. Res.* **1986**, *19*, 162. (b) Scandola, F.; Bignozzi, C. A.; Chiorboli, C.; Indelli, M. T.; Rampi, M. A. *Coord. Chem. Rev.* **1990**, *97*, 299. (c) Pfennig, B. W.; Bocarsly, A. B. *Coord. Chem. Rev.* **1991**, *111*, 91. (d) Scandola, F.; Argazzi, R.; Bignozzi, C. A.; Chiorboli, C.; Indelli, M. T.; Rampi, M. A. *Coord. Chem. Rev.* **1993**, *125*, 283. (e) Wu, Y.; Pfennig, B. W.; Sharp, S. L.; Ludwig, D. R.; Warren, C. J.; Vicenzi, E. P.; Bocarsly, A. B. *Coord. Chem. Rev.* **1997**, *159*, 245. (f) Ouahab, L. *Coord. Chem. Rev.* **1998**, *178−180*, 1501. (g) Verdaguer, M.; Bleuzen, A.; Marvaud, V.; Vaissermann, J.; Seuleiman, M.; Desplanches, C.; Scuiller, A.; Train, C.; Garde, R.; Gelly, G.; Lomenech, C.; Rosenman, I.; Veillet, P.; Cartier, C.; Villain, F. *Coord. Chem. Rev.* **1999**, *190−192*, 1023. (h) Chang, C. C.; Pfennig, B.; Bocarsly, A. B. *Coord. Chem. Rev.* **2000**, *208*, 33. (i) Miller, J. S.; Manson, J. L. *Acc. Chem. Res.* **2001**, *34*, 563. (j) Černák, J.; Orendáč, M.; Potočňák, I.; Chomič, J.; Orendáčová, A.; Skoršepa, J.; Feher, A. *Coord. Chem. Rev.* **2002**, *224*, 51. (k) Plečnik, C. E.; Liu, S.; Shore, S. G. *Acc. Chem. Res.* **2003**, *36*, 499.

10.1021/ic800743a CCC: $40.75
Published on Web 10/14/2008

electronic and magnetic properties over the past decades,[3] and new materials with unprecedented properties continue unabated.[4]

Cyanide ligand in a linear coordination mode, like its isoelectronic relatives C≡O and $^{-}$C≡CR, interacts with the metal ion through σ-bonding and π-back-bonding interaction(s),[5] depending upon the metal ion and auxiliary ligand. The bonding interaction between metal ions and $^{-}$C≡N provides the mean for electronic communication in cyanide-linked multinuclear complexes, in both the ground and excited states. However, spectroscopic studies and theoretical calculations on metal−cyanide complexes of second and third row transition metal ions are sparse in the literature.[6] The ubiquitous incorporation of unsaturated organic ancillary ligands in most literature-reported metal−cyanide complexes hampers spectral assignment and interpretation of the electronic transitions.

Several years ago, we initiated a research program on organoruthenium complexes containing the macrocyclic tertiary amine ligand 1,5,9,13-tetramethyl-1,5,9,13-tetraazacyclohexadecane (16-TMC).[7] This ligand is optically transparent in the UV−visible spectral region and is suited to allow examination of electronic transitions associated with Ru−C≡N fragment. Furthermore, 16-TMC is a σ donor and does not compete with $^{-}$C≡N ligand for π-bonding interactions. Bis-(cyano) metal complexes of 16-TMC should adopt a trans configuration and are a useful building block for the construction of 1-D $-[N\equiv C-RuL_4-C\equiv N-M]_n-$ solids. Previously, we have reported the structural, spectroscopic, and electrochemical properties of *trans*-[Ru(16-TMC)(C≡CAr)$_2$]$^{n+}$ (n = 0 or 1)[7a,e] and *trans*-[Ru(16-TMC)(C≡N^{t}Bu)$_2$]$^{2+}$.[7c] Herein is described the structures and spectroscopic and electrochemical properties of bis(cyanide) ruthenium(II) and -(III) complexes supported by 16-TMC ligand. Resonance Raman spectroscopy has been utilized to probe the electronic transition(s) associated with the [N≡C−Ru−C≡N] moiety in order to gain insight into the Ru−C≡N bonding interaction. Density functional theory (DFT) and time-dependent-DFT (TD-DFT) calculations have been performed on the model complexes *trans*-[(NH$_3$)$_4$Ru(C≡N)$_2$] and *trans*-[(NH$_3$)$_4$Ru(C≡N)$_2$]$^{+}$ to examine the Ru−cyanide interaction and the nature of the associated electronic transition(s).

Experimental Section

General Procedures. All reactions were performed under an argon atmosphere using standard Schlenk techniques. Solvents were dried by standard methods and distilled before use. *trans*-[Ru(16-TMC)Cl$_2$]Cl (16-TMC = 1,5,9,13-tetramethyl-1,5,9,13-tetraazacyclohexadecane) was prepared by a published procedure.[8] Zinc powder (BDH), bromine, ammonium hexafluorophosphate, and potassium cyanide (Aldrich) were used as received unless otherwise stated. In the ^{1}H and ^{13}C{^{1}H} NMR spectra, multiple resonances corresponding to different conformations of 16-TMC were observed. In the literature, it has been reported that the 16-TMC ligand, like its 14- and 15-TMC congeners, can exhibit several possible conformations upon coordination to a metal ion.[9] In the ^{1}H NMR spectrum of **1**, all signals of the coordinated 16-TMC ligand have been assigned. Fast atom bombardment (FAB) mass spectra were obtained on a Finnigan MAT 95 mass spectrometer with a 3-nitrobenzyl alcohol matrix. Infrared spectra were recorded as nujol mulls or KBr pellets on a Bio-Rad FT-IR spectrometer. UV−visible absorption spectra were recorded on a Perkin-Elmer Lambda 19 spectrophotometer. Elemental analyses were performed by Butterworth Laboratories Ltd., Teddington, United Kingdom. A conventional two-compartment electrochemical cell was used in cyclic voltammetry experiments. A Ag/AgNO$_3$ (0.1 M in CH$_3$CN) electrode was used as the reference electrode. All solutions were degassed with argon before electrochemical measurements. $E_{1/2}$ values were taken from the average of the cathodic and anodic peak potentials for the oxidative and reductive waves. A ferrocenium/ferrocene couple ($FeCp_2^{+/0}$) was used as an internal reference.

Synthesis. *trans*-[Ru(16-TMC)(C≡N)$_2$] (1). A mixture of *trans*-[Ru(16-TMC)Cl$_2$]Cl (0.10 g, 0.2 mmol) and zinc powder (0.20 g, 3.1 mmol) in methanol (20 cm^3) was refluxed for 30 min. An aqueous solution (5 cm^3) of KCN (0.10 g, 1.5 mmol) was added, and the resulting mixture was stirred at 50 °C for 18 h. After cooling, all volatiles were removed in vacuo. The product was extracted into CH_2Cl_2, and the solvent was removed in vacuo. A pale yellow crystalline solid was obtained by the diffusion of diethyl ether into a dichloromethane solution. Yield = 0.05 g (57%). Anal. calcd for $C_{18}H_{36}N_6Ru$: C, 49.29; H, 8.28; N, 19.17. Found: C, 49.37; H, 8.27; N, 19.16. ^{1}H NMR (270 MHz, CD_2Cl_2): 1.44−1.90 (m,

(3) (a) Dunbar, K. M.; Heintz, R. A. *Prog. Inorg. Chem.* **1997**, *45*, 283. (b) Ohba, M.; Ōkawa, H. *Coord. Chem. Rev.* **2000**, *198*, 313.

(4) For recent works, see: (a) Mironov, Y. V.; Virovets, A. V.; Artemkina, S. B.; Fedorov, V. E. *Angew. Chem., Int. Ed.* **1998**, *37*, 2507. (b) Naumov, N. G.; Virovets, A. V.; Sokolov, M. N.; Artemkina, S. B.; Fedorov, V. E. *Angew. Chem., Int. Ed.* **1998**, *37*, 1943. (c) Niu, T.; Wang, X.; Jacobson, A. J. *Angew. Chem., Int. Ed.* **1999**, *38*, 1934. (d) Holmes, S. M.; Girolami, G. S. *J. Am. Chem. Soc.* **1999**, *121*, 5593. (e) Ma, B.-Q.; Gao, S.; Su, G.; Xu, G.-X. *Angew. Chem., Int. Ed.* **2001**, *40*, 434. (f) Inoue, K.; Kikuchi, K.; Ohba, M.; Ōkawa, H. *Angew. Chem., Int. Ed.* **2003**, *42*, 4810. (g) Margadonna, S.; Prassides, K.; Fitch, A. N. *J. Am. Chem. Soc.* **2004**, *126*, 15390. (h) Kaye, S. S.; Long, J. R. *J. Am. Chem. Soc.* **2005**, *127*, 6506. (i) Chapman, K. W.; Chupas, P. J.; Kepert, C. J. *J. Am. Chem. Soc.* **2005**, *127*, 15630. (j) Goodwin, A. L.; Chapman, K. W.; Kepert, C. J. *J. Am. Chem. Soc.* **2005**, *127*, 17980. (k) Cobo, S.; Molnár, G.; Real, J. A.; Bousseksou, A. *Angew. Chem., Int. Ed.* **2006**, *45*, 5786. (l) Kaneko, W.; Kitagawa, S.; Ohba, M. *J. Am. Chem. Soc.* **2007**, *129*, 248. (m) Yanai, N.; Kaneko, W.; Yoneda, K.; Ohba, M.; Kitagawa, S. *J. Am. Chem. Soc.* **2007**, *129*, 3496. (n) Kaneko, W.; Ohba, M.; Kitagawa, S. *J. Am. Chem. Soc.* **2007**, *129*, 13706.

(5) (a) Nast, R. *Coord. Chem. Rev.* **1982**, *47*, 89. (b) Manna, J.; John, K. D.; Hopkins, M. D. *Adv. Organomet. Chem.* **1995**, *38*, 79.

(6) (a) Gray, H. B.; Beach, N. A. *J. Am. Chem. Soc.* **1963**, *85*, 2922. (b) Alexander, J. J.; Gray, H. B. *J. Am. Chem. Soc.* **1968**, *90*, 4260. (c) Mason, W. R. *J. Am. Chem. Soc.* **1973**, *95*, 3573. (d) Mason, W. R. *J. Am. Chem. Soc.* **1976**, *98*, 5182. (e) Pierloot, K.; Praet, E. V.; Vanquickenborne, L. G.; Roos, B. O. *J. Phys. Chem.* **1993**, *97*, 12220. (f) Rawashdeh-Omary, M. A.; Omary, M. A.; Patterson, H. H. *J. Am. Chem. Soc.* **2000**, *122*, 10371.

(7) (a) Choi, M.-Y.; Chan, M. C.-W.; Zhang, S.; Cheung, K.-K.; Che, C.-M.; Wong, K.-Y. *Organometallics* **1999**, *18*, 2074. (b) Choi, M.-Y.; Chan, M. C. W.; Peng, S.-M.; Cheung, K.-K.; Che, C.-M. *Chem. Commun.* **2000**, 1259. (c) Lee, F.-W.; Choi, M.-Y.; Cheung, K.-K.; Che, C.-M. *J. Organomet. Chem.* **2000**, *595*, 114. (d) Wong, C.-Y.; Che, C.-M.; Chan, M. C. W.; Leung, K.-H.; Phillips, D. L.; Zhu, N. *J. Am. Chem. Soc.* **2004**, *126*, 2501. (e) Wong, C.-Y.; Che, C.-M.; Chan, M. C. W.; Han, J.; Leung, K.-H.; Phillips, D. L.; Wong, K.-Y.; Zhu, N. *J. Am. Chem. Soc.* **2005**, *127*, 13997. (f) Wong, C.-Y.; Tong, G. S. M.; Che, C.-M.; Zhu, N. *Angew. Chem., Int. Ed.* **2006**, *45*, 2694–2698.

(8) Che, C.-M.; Wong, K.-Y.; Poon, C.-K. *Inorg. Chem.* **1986**, *25*, 1809.

(9) (a) Che, C.-M.; Wong, K.-Y.; Mak, T. C. W. *Chem. Commun.* **1985**, 546. (b) Mak, T. C. W.; Che, C.-M.; Wong, K.-Y. *Chem. Commun.* **1985**, 986. (c) Che, C.-M.; Wong, K.-Y.; Mak, T. C. W. *Chem. Commun.* **1985**, 988. (d) Che, C.-M.; Cheng, W.-K.; Lai, T.-F.; Poon, C.-K.; Mak, T. C. W. *Inorg. Chem.* **1987**, *26*, 1678. (e) Che, C.-M.; Lai, T.-F.; Wong, K.-Y. *Inorg. Chem.* **1987**, *26*, 2289.

16H, NCH_2), 2.57 (s, 12H, NCH_3), 3.63−3.75 (m, 8H, CH_2). ^{13}C{^{1}H} NMR (68 MHz, CD_2Cl_2): 22.0 (NCH$_2$CH_2), 51.0 (NCH_3), 61.2, 69.1 (NCH_2), 171.5 (CN). Infrared (nujol, cm^{-1}): 2031 ν(C≡N). FAB-MS (*m*/*z*): 438, [M]$^+$.

***trans*-[Ru(16-TMC)(C≡N)$_2$]PF$_6$ (2·PF$_6$).** A solution of bromine (0.47 g, 2.9 mmol) in dichloromethane (ca. 5 cm^3) was added dropwise to a solution of *trans*-[Ru(16-TMC)(CN)$_2$] (0.048 g, 0.11 mmol) in dichloromethane (10 cm^3). After stirring for 10 min, the yellow precipitate formed was collected by filtration, washed with dichloromethane (5 cm^3 × 3), and dried in the air. The product was dissolved in water and filtered. The addition of ammonium hexafluorophosphate afforded a yellow precipitate which was filtered and dried in the air. Recrystallization by the diffusion of diethyl ether into an acetonitrile solution gave yellow crystals. Yield = 0.054 g (84%). Anal. calcd for $C_{18}H_{36}F_6N_6PRu$: C, 37.04; H, 6.22; N, 14.41. Found: C, 37.20; H, 6.18; N, 14.40. Infrared (KBr, cm^{-1}): 2101 ν(C≡N). FAB-MS (*m*/*z*): 438, [M]$^+$.

Resonance Raman Spectroscopy. Sample solutions of *trans*-[Ru(16-TMC)(C≡N)$_2$] with concentrations of 1.1−1.2 mM were prepared using a spectroscopic-grade methanol solvent. The methods and apparatus used for the resonance Raman experiments have previously been described,[10] and only a summary is given here. The harmonics of a Nd:YAG laser and their hydrogen Raman shifted laser lines were the source of the excitation frequencies for the resonance Raman experiments. A stirred cell sample or flowing liquid jet sample was excited by a moderately focused laser beam. A backscattering geometry and reflective optics were used to collect the Raman light and image it through a depolarizer and entrance slit of a 0.5 m spectrograph. The grating of the spectrograph dispersed the Raman signal onto a liquid-nitrogen-cooled CCD detector which acquired the signal for 60−120 s before being read out to an interfaced PC. About 30−60 of these readouts were added to find the resonance Raman spectrum. The known vibrational frequencies of the solvent Raman bands were used to calibrate the Raman shift wavenumbers of the Raman spectra. Reabsorption of the Raman light by the sample was corrected for using methods previously described.[11] The Raman spectra were also corrected for the wavelength response of the detection system using an intensity calibrated deuterium lamp. Solvent bands were removed by subtracting an appropriately scaled solvent spectrum from the resonance Raman spectrum. The integrated areas of the resonance Raman bands were found by fitting a baseline plus a sum of Lorentzians to portions of the spectrum. The concentrations of the sample solutions before and after the absolute Raman cross-section measurements were found spectrophotometrically, and changes of less than 5% were seen (presumably due to solvent evaporation and sample degradation). The means of three trials at each excitation wavelength were used to determine the absolute Raman cross sections, which were measured relative to the methanol solvent cross section. The methanol solvent Raman cross section was determined relative to the dichloromethane solvent cross section, which was found relative to previously measured cyclohexane.[12] The maximum molar extinction coefficient for *trans*-[Ru(16-TMC)(C≡N)$_2$] in methanol was measured to be 17 560 dm^3 mol^{-1} cm^{-1}.

X-Ray Crystallography. Crystals of **1**·2H$_2$O or **2**·PF$_6$·H$_2$O were obtained by the diffusion of diethyl ether into dichloromethane or acetonitrile solution, respectively. The crystals were mounted on a glass fiber, and diffraction data were collected at 301 K on a Rigaku AFC7R diffractometer using graphite monochromatized Mo K$_\alpha$ radiation (λ = 0.71073 Å). Structures of **1**·2H$_2$O and **2**·PF$_6$·H$_2$O were solved by direct methods employing the SHELXS-97 program[13] on a PC. Ru and many non-H atoms were located according to the direct methods. The position of the other non-hydrogen atoms were found after successful refinement by full-matrix least-squares using the SHELXL-97[13] program on a PC. For both **1**·2H$_2$O and **2**·PF$_6$·H$_2$O, one crystallographic asymmetric unit consists of half of one formula unit, and the Ru atoms are at the special position. In the final stage of least-squares refinement, all non-H atoms were refined anisotropically. The positions of H atoms (except those on water O) were calculated on the basis of the riding mode with thermal parameters equal to 1.2 times those of the associated C atoms, and participated in the calculation of final *R* indices. In **2**·PF$_6$·H$_2$O, C atoms (C(3), C(4), and C(8)) bonded to the N(2) atom were unequally disordered by flip with a ratio of 0.694:0.306. Meanwhile, C(2) and C(5) were slightly disordered into two sets of positions.

Computational Methodology. DFT calculations were performed on *trans*-[(NH$_3$)$_4$Ru(C≡N)$_2$] (**1′**, with C_{2v} symmetry imposed) and *trans*-[(NH$_3$)$_4$Ru(C≡N)$_2$]$^+$ (**2′**, without symmetry constraint), which were used as models for the ruthenium complexes studied in this work. In each case, direction along the N≡C−Ru−C≡N is defined to coincide with the *z* axis of the coordinate system, and the Ru−N bonds in the *x* and *y* directions. The C_{2v} symmetry was employed in the calculations for **1′** because it can provide a simple model to interpret the nature/pseudosymmetry of the molecular orbitals. The same approach has previously been employed in the DFT/TD-DFT calculations on *trans*-[Ru(NH$_3$)$_4$(C≡CR)$_2$], which was used to model complexes *trans*-[Ru(16-TMC)(C≡CR)$_2$],[7e] and the calculated vertical electronic transitions were in good agreement with the corresponding experimental data. Moreover, the symmetry-unrestrained DFT/TD-DFT calculations were performed on **1′**, and the corresponding calculated spectrum and molecular orbital compositions were presented in the Supporting Information (Figure S4 and Table S5, respectively). As there is no significant difference in the results of calculation on the C_{2v} and symmetry-unrestrained (C_1) **1′**, the use of C_{2v} symmetry is justified. The electronic ground states of **1′** and **2′** were optimized using the restricted and unrestricted density functional HCTH/147, respectively.[14] As the electronic transitions of the complexes studied in this work are in the high-energy ultraviolet region, the HCTH functional was chosen because many conventional functionals break down in the calculations of high-lying or Rydberg excited states, whereas the family of HCTH functionals were designed to tackle such deficiency. The Stuttgart small-core relativistic effective core potential was employed for Ru atoms with its accompanying basis set.[15a] For all other atoms, the 6-31G* basis set was employed.[15b,c] The vertical transition energies of both model complexes were computed in CH_3CN at the respective gas-phase-optimized ground-state geometry using the TD-DFT method. The conductor polarizable continuum model (CPCM) was used to account for solvent effects on the electronic transitions.[16] As the solvent used in the resonance Raman experiments was MeOH, the UV−visible absorption spectrum of **1′** in MeOH has also been calculated, and the calculated

(10) Zheng, X.; Phillips, D. L. *J. Chem. Phys.* **1998**, *108*, 5772.
(11) Myers, A. B.; Li, B.; Ci, X. *J. Chem. Phys.* **1988**, *89*, 1876.
(12) (a) Trulson, M. O.; Dollinger, G. D.; Mathies, R. A. *J. Chem. Phys.* **1989**, *90*, 4274. (b) Kwok, W. M.; Phillips, D. L.; Yeung, P. K.-Y.; Yam, V. W.-W. *J. Phys. Chem. A* **1997**, *101*, 9286.
(13) Sheldrick, G. M. *SHELX97*, release 97-2; University of Goetingen: Goetingen, Germany, 1997.
(14) Boese, A. D.; Doltsinis, N. L.; Handy, N. C.; Sprik, M. *J. Chem. Phys.* **2000**, *112*, 1670.
(15) (a) Andrae, D.; Haeussermann, U.; Dolg, M.; Stoll, H.; Preuss, H. *Theor. Chim. Acta* **1990**, *77*, 123. (b) Hariharan, P. C.; Pople, J. A. *Theor. Chim. Acta* **1973**, *28*, 213. (c) Francl, M. M.; Petro, W. J.; Hehre, W. J.; Binkley, J. S.; Gordon, M. S.; Defree, D. J.; Pople, J. A. *J. Chem. Phys.* **1982**, *77*, 3654.
(16) Barone, V.; Cossi, M. *J. Phys. Chem. A* **1998**, *102*, 1995.

Scheme 1

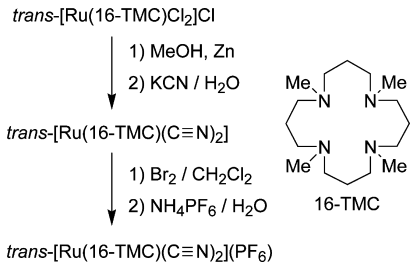

spectrum and molecular orbital compositions were depicted in the Supporting Information (Figure S5 and Table S6, respectively). The natures of the electronic transitions of **1′** in both solvents are essentially the same, although there is a slight difference in the transition energies, and this is attributed to the change of polarization on the solvent model. Tight self-consistent field convergence (10^{-8} au) was used for all calculations. The calculations were performed using the Gaussian 03 program package.[17]

Results

Synthesis and Characterization. Reaction of *trans*-[Ru(16-TMC)Cl_2]Cl with KCN in the presence of zinc powder (as reducing agent) afforded complex **1**, *trans*-[Ru(16-TMC)(C≡N)$_2$], as a pale yellow solid (Scheme 1). Oxidation of **1** by bromine in CH_2Cl_2 gave **2**, *trans*-[Ru(16-TMC)(C≡N)$_2$]$^+$, isolated as a yellow PF_6^- salt. Attempts to synthesize **2** by reacting *trans*-[Ru(16-TMC)Cl_2]Cl with KCN in methanol were not successful; presumably the chloride ligands of *trans*-[Ru(16-TMC)Cl_2]$^+$ are not reactive toward substitution reaction. The ^{1}H NMR signals of the 16-TMC ligand in **1** are similar to those observed for *trans*-[Ru(16-TMC)(C≡CAr)$_2$][7a,e] and *trans*-[Ru(16-TMC)-(C≡N^{t}Bu)$_2$](ClO_4)$_2$.[7c] The ^{13}C{^{1}H} NMR signal at 171.5 ppm for **1**, together with its $\nu_{C\equiv N}$ stretching frequency at 2031 cm^{-1}, confirm the presence of the C≡N ligand. The $\nu_{C\equiv N}$ for **2** is 2101 cm^{-1}, which is higher than that of **1** by 70 cm^{-1}.

X-Ray Crystallography. Figures 1 and 2 show the perspective views of **1** and **2**, respectively. Crystallographic data for both complexes are listed in Table 1. The ruthenium atoms in both cases reside in a pseudo-octahedral environment, with the two C≡N ligands trans to each other. The six-membered chelate rings of the Ru(16-TMC) moiety are individually in a chair conformation with the N-methyl groups adopting the "two up, two down" configuration, as in *trans*-[Ru(16-TMC)(C≡N^{t}Bu)$_2$](ClO_4)$_2$[7c] and *trans*-[Ru(16-

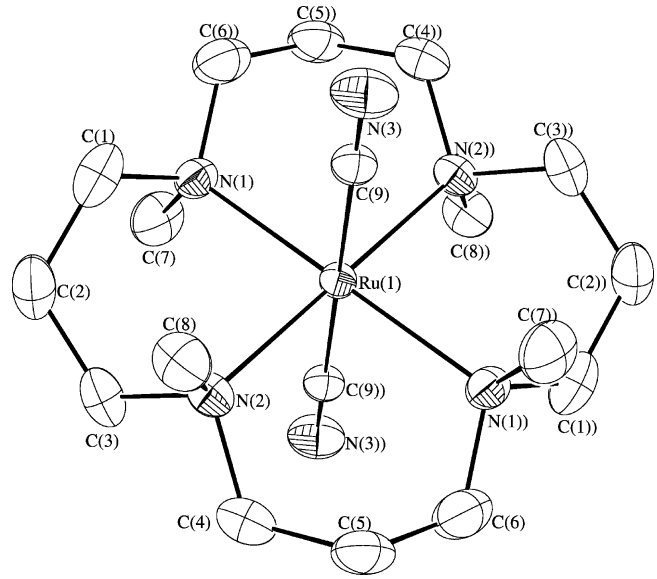

Figure 1. Perspective view of **1** (40% probability ellipsoids). Selected bond lengths (Å) and angles (deg): Ru−C(9), 2.061(4); C(9)−N(3), 1.130(5); Ru−N(1), 2.269(3); Ru−N(2), 2.271(3); Ru−C(9)−N(3), 178.7(4).

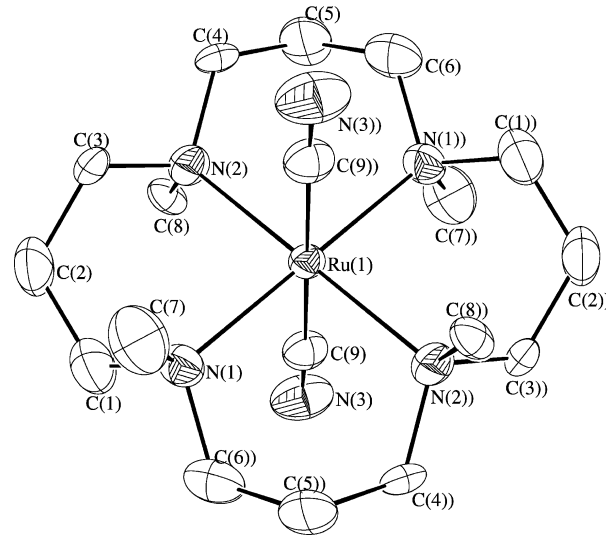

Figure 2. Perspective view of **2** (40% probability ellipsoids). Selected bond lengths (Å) and angles (deg): Ru−C(9), 2.069(5); C(9)−N(3), 1.140(7); Ru−N(1), 2.251(4); Ru−N(2), 2.243(4); Ru−C(9)−N(3), 177.5(5).

Table 1. X-Ray Crystallographic Data for **1** and **2**

complex	**1**·2H_2O	**2**·PF_6·H_2O
formula	$C_{18}H_{36}N_6Ru$·2H_2O	$C_{18}H_{36}N_6RuPF_6$·H_2O
fw	473.63	600.58
space group	*Pccn* (No. 56)	*C*2/*c* (No. 15)
a, Å	13.230(2)	22.722(4)
b, Å	14.983(2)	12.625(2)
c, Å	10.712(1)	10.199(2)
β, deg	90	116.25(2)
V, Å^3	2123.4(5)	2624.0(8)
Z	4	4
T, K	301(2)	301(2)
λ, Å	0.71073	0.71073
D_c, g cm^{-3}	1.482	1.520
μ, cm^{-1}	7.64	7.23
R, R_w[a]	0.030, 0.096	0.044, 0.139

[a] $R = \sum||F_o| - |F_c||/\sum|F_o|$. $wR = \{\sum[w(F_o^2 - F_c^2)^2]/\sum[w(F_o^2)^2]\}^{1/2}$.

(17) Frisch, M. J.; Trucks, G. W.; Schlegel, H. B.; Scuseria, G. E.; Robb, M. A.; Cheeseman, J. R.; Montgomery, J. A., Jr.; Vreven, T.; Kudin, K. N.; Burant, J. C.; Millam, J. M.; Iyengar, S. S.; Tomasi, J.; Barone, V.; Mennucci, B.; Cossi, M.; Scalmani, G.; Rega, N.; Petersson, G. A.; Nakatsuji, H.; Hada, M.; Ehara, M.; Toyota, K.; Fukuda, R.; Hasegawa, J.; Ishida, M.; Nakajima, T.; Honda, Y.; Kitao, O.; Nakai, H.; Klene, M.; Li, X.; Knox, J. E.; Hratchian, H. P.; Cross, J. B.; Bakken, V.; Adamo, C.; Jaramillo, J.; Gomperts, R.; Stratmann, R. E.; Yazyev, O.; Austin, A. J.; Cammi, R.; Pomelli, C.; Ochterski, J. W.; Ayala, P. Y.; Morokuma, K.; Voth, G. A.; Salvador, P.; Dannenberg, J. J.; Zakrzewski, V. G.; Dapprich, S.; Daniels, A. D.; Strain, M. C.; Farkas, O.; Malick, D. K.; Rabuck, A. D.; Raghavachari, K.; Foresman, J. B.; Ortiz, J. V.; Cui, Q.; Baboul, A. G.; Clifford, S.; Cioslowski, J.; Stefanov, B. B.; Liu, G.; Liashenko, A.; Piskorz, P.; Komaromi, I.; Martin, R. L.; Fox, D. J.; Keith, T.; Al-Laham, M. A.; Peng, C. Y.; Nanayakkara, A.; Challacombe, M.; Gill, P. M. W.; Johnson, B.; Chen, W.; Wong, M. W.; Gonzalez, C.; Pople, J. A. *Gaussian 03*, revision D.01; Gaussian, Inc.: Wallingford, CT, 2004.

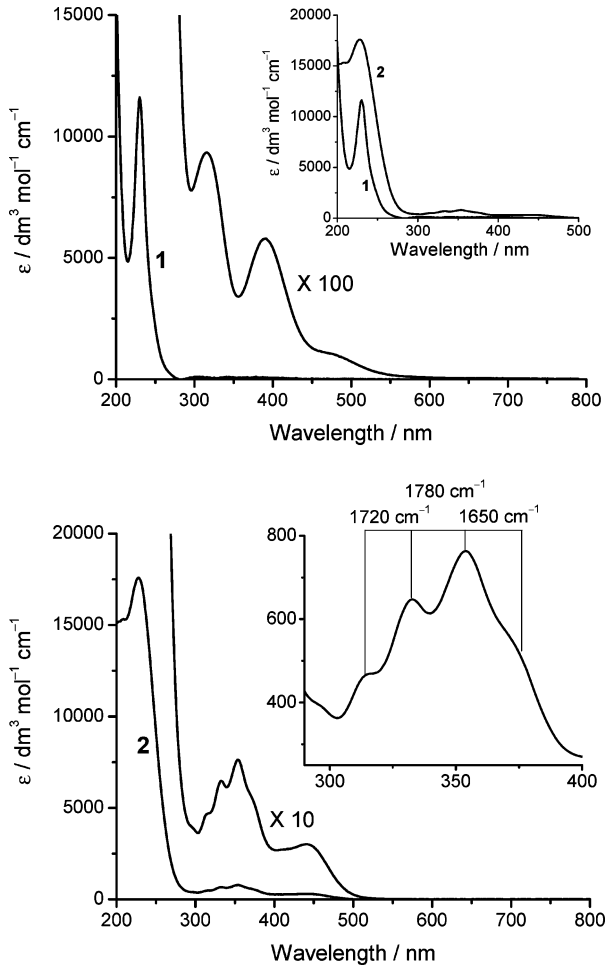

Figure 3. UV−vis absorption spectra of **1** and **2** in CH_3CN at 298 K. Inserted figures: (top) overlay for **1** and **2** in the high-energy region; (bottom) enlarged view for the weak absorptions for **2**.

TMC)(C≡CAr)$_2$].[7a,b] The Ru−C/C−N distances in **1** and **2** are 2.061(4)/1.130(5) and 2.069(5)/1.140(7) Å, respectively, which are insensitive to the oxidation state of the ruthenium atom despite the significant difference in the $\nu_{C\equiv N}$ values of **1** and **2**.

Electrochemistry. Electrochemistry was examined with acetonitrile solutions of the ruthenium complexes by cyclic voltammetry. A reversible couple at $E_{1/2} = +0.10$ V versus $FeCp_2^{+/0}$ was observed for both **1** and **2**. As the peak current is comparable to that of the $FeCp_2^{+/0}$ couple measured at the same concentration, a one-electron electrochemical process is suggested, and the reversible redox couple is assigned to the Ru(III)/(II) couple.

Absorption Spectroscopy. The absorption spectra of **1** and **2** are depicted in Figure 3. Complex **1** exhibits an intense high-energy absorption band at $\lambda_{max} = 230$ nm ($\varepsilon_{max} = 11\,610$ dm^3 mol^{-1} cm^{-1}), with weak absorptions at $\lambda_{max} = 316$, 389, and 490 (shoulder (sh)) nm ($\varepsilon_{max} =$ 90, 60, and 10 dm^3 mol^{-1} cm^{-1}, respectively). Complex **2** features strong high-energy absorptions where a peak maximum at $\lambda_{max} = 228$ nm ($\varepsilon_{max} = 17\,590$ dm^3 mol^{-1} cm^{-1}) with tailing to 290 nm is recorded; weak bands with peak maxima at 315 (sh), 333, 354, 376 (sh), and 441 nm ($\varepsilon_{max} = 470$, 650, 760, 520, and 300 dm^3 mol^{-1} cm^{-1}, respectively) are also observed. It is noted that the

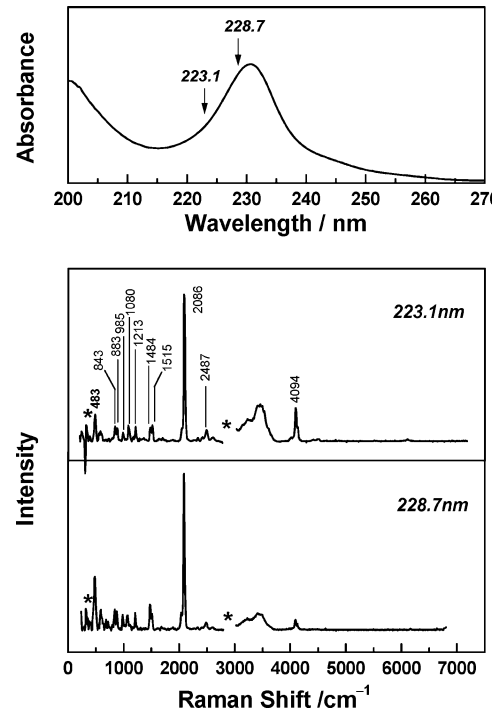

Figure 4. (Top) Electronic absorption spectrum of *trans*-[Ru(16-TMC)(C≡N)$_2$] (**1**) in methanol with the excitation wavelengths for the resonance Raman experiments indicated above the spectrum. (Bottom) Resonance Raman spectra of **1** obtained with 223.1 and 228.7 nm excitation wavelength in methanol at 25 °C (solvent and laser subtraction artifacts marked by ∗).

spacings between adjacent peak maxima in the 315−376 nm spectral region are 1720, 1780, and 1650 cm^{-1}, which could be correlated to $\nu_{C\equiv N}$ in the electronic excited state.

Resonance Raman Spectroscopy. Figure 4 presents an absorption spectrum of *trans*-[Ru(16-TMC)(C≡N)$_2$] (**1**) in a methanol solution and an overview of the 223.1 and 228.7 nm resonance Raman spectra. The resonance Raman spectra depicted in Figure 4 have been intensity-corrected, solvent-subtracted, and background-subtracted. Nine fundamental bands (at 483, 843, 883, 985, 1080, 1213, 1484, 1515, and 2086 cm^{-1}) and their overtones/combination bands (2487 and 4094 cm^{-1}) account for most of the intensity in the resonance Raman spectra. The largest mode is the nominal C≡N stretch at 2086 cm^{-1}, and this vibrational mode has significant intensity in its overtone at 4094 cm^{-1} and its combination band with the 483 cm^{-1} mode (∼2487 cm^{-1}). In order to determine the individual mode internal reorganization energies (λ), which are defined as the energy difference between the equilibrium geometries of the electronic excited and ground states, the absorption spectrum and resonance Raman intensity data were analyzed by a methodology employed in a number of our previous studies.[7d,e,18] The typical simulation procedures are (1) initial estimation of the geometry change along the Raman-active modes accompanying electronic excitation and (2) refinement on the

(18) (a) Leung, K. H.; Phillips, D. L.; Tse, M.-C.; Che, C.-M.; Miskowski, V. M. *J. Am. Chem. Soc.* **1999**, *121*, 4799. (b) Che, C.-M.; Tse, M.-C.; Chan, M. C. W.; Cheung, K. K.; Phillips, D. L.; Leung, K.-H. *J. Am. Chem. Soc.* **2000**, *122*, 2464. (c) Che, C.-M.; Mao, Z.; Miskowski, V. M.; Tse, M.-C.; Chan, C.-K.; Cheung, K.-K.; Phillips, D. L.; Leung, K.-H. *Angew. Chem., Int. Ed.* **2000**, *39*, 4084.

Table 2. Resonance Raman Bands of *trans*-[Ru(16-TMC)(C≡N)$_2$] (**1**) in Methanol

Raman band	Raman shift[a]/cm^{-1}	absolute Raman cross section/10^{-7} Å^2/molecule			
		223.1 nm		228.7 nm	
		exptl.[b]	calcd.	exptl.[b]	calcd.
fundamental	483	0.25	0.29	1.20	1.20
fundamental	843	0.11	0.12	0.31	0.29
fundamental	883	0.10	0.10	0.21	0.24
fundamental	985	0.08	0.09	0.19	0.19
fundamental	1080	0.15	0.15	0.26	0.27
fundamental	1213	0.11	0.11	0.18	0.18
fundamental	1484	0.13	0.12	0.40	0.22
fundamental	1515	0.09	0.11	0.20	0.13
fundamental	2086	1.50	1.91	3.11	1.83
combination (2086 + 483)	2487	0.15	0.09	0.19	0.11
overtone (2 × 2086)	4094	0.23	0.23	0.17	0.10

[a] Estimated uncertainties are about 4 cm^{-1} for the Raman shifts. [b] Estimated uncertainties are about 10% for intensities 0.5 × 10^{-7} Å^2/molecule and higher, 20% for intensities between 0.1 and 0.5 × 10^{-7} Å^2/molecule, and 50% for intensities lower than 0.10 × 10^{-7} Å^2/molecule.

Table 3. Parameters for Simulations of Resonance Raman Intensities and Absorption Spectrum of *trans*-[Ru(16-TMC)(C≡N)$_2$] (**1**)[a]

ground state vibrational frequency/cm^{-1}	excited state vibrational frequency/cm^{-1}	Δ[b]	vibrational reorganizational energy/cm^{-1}
483	483	0.396	38
843	843	0.151	10
883	883	0.136	8
985	985	0.121	7
1080	1080	0.143	11
1213	1213	0.115	8
1484	1484	0.132	13
1515	1515	0.103	8
2086	2086	0.435	197

[a] Total vibrational reorganizational energies, $\lambda_v = 300$; zero−zero energy of the electronic transition, $E_0 = 43\,260$ cm^{-1}; transition length, $M = 0.737$ Å; solution refractive index, $n = 1.327$; homogeneous broadening, $\Gamma = 300$ cm^{-1} HWHM; inhomogeneous broadening, $G = 675$ cm^{-1} standard deviation. [b] Displacement between equilibrium nuclear configurations of excited state and ground state in ground-state dimensionless coordinates.

geometry changes through direct computation of the absorption spectra and Raman excitation profiles via a time-dependent wavepacket approach. The final values of the geometry changes (Δ, in dimensionless coordinates) obtained from these calculations are related to the single-mode internal reorganization energies. Table 2 lists the Raman band positions and Raman cross sections for the resonance Raman spectra excited at 223.1 and 228.7 nm (Figure 4). The best fit parameters used to simulate the resonance Raman cross sections and absorption spectrum are summarized in Table 3. Figure 5 depicts a graphical comparison of the calculated and experimental absorption spectra and resonance Raman cross sections for **1**. The calculated absorption spectrum and resonance Raman cross sections exhibit reasonable agreement with the experimental values. Since we have no data about the values of the excited-state vibrational frequencies for **1**, we assumed no change in the vibrational frequency, although it is most likely that the excited-state vibrational frequencies are somewhat different than those in the ground state. This approximation is reasonable since the total reorganizational energy is fairly small (on the order of 300 cm^{-1}) and is distributed over a number of modes. Since the C≡N stretch mode that has most of the vibrational reorganizational energy has a high frequency of 2086 cm^{-1}, even a change of a bond

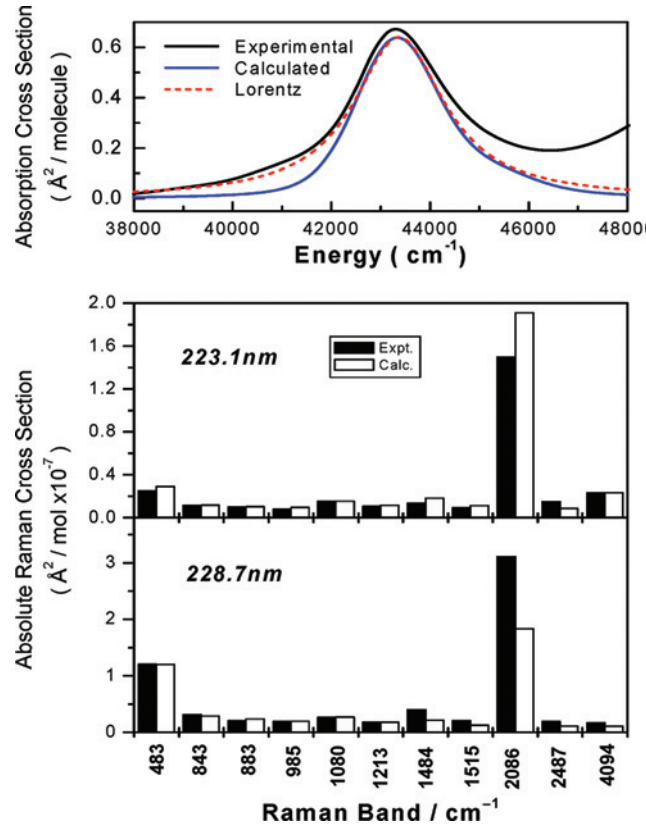

Figure 5. (Top) Comparison of the calculated (blue line) and experimental (black line) electronic absorption spectra of **1**. (Bottom) Comparison of the calculated (open bars) and experimental (solid bars) resonance Raman cross sections for the 223.1 and 228.7 nm resonance Raman spectra of **1**. The calculations used the parameters given in Table 3 and the model described in references for the simple exponential decay dephasing description of the solvent.[19]

order from 3 to 2.5 will probably change the vibrational frequency in the excited state by only a moderate amount (maybe 100 or 200 cm^{-1}) and not dramatically change the value of Δ (in dimensionless coordinates) estimated from using the approximation of no change in the vibrational frequency for the vibrational modes. The somewhat anomalous behavior of the C≡N stretch at a 2086 cm^{-1} fundamental intensity as a function of the wavelength could be due to preresonant−resonant interference, which usually affects fundamental bands much more strongly than combination bands or overtones[19] or a moderately reduced vibrational frequency in the excited-state versus the ground-state frequency for this mode. We note that there is better agreement between the calculated and experimental cross sections for the combination band and overtone of the 2086 cm^{-1} mode (at 2487 cm^{-1} and 4094 cm^{-1}, respectively) than the fundamental. This is consistent with some preresonant−resonant interference perturbing the 2086 cm^{-1} fundamental cross section. Most of the vibrational reorganizational energy (ca. 66% of the total) and displacement is along the nominal C≡N stretch in the excited state relative to the ground state.

DFT and TD-DFT Calculations. The ground-state structures of the model complexes *trans*-[(NH$_3$)$_4$Ru(C≡N)$_2$] (**1′**)

(19) (a) Phillips, D. L.; Myers, A. B. *J. Chem. Phys.* **1991**, *95*, 226. (b) Kwok, W. M.; Phillips, D. L. *J. Chem. Phys.* **1996**, *104*, 9816. (c) Phillips, D. L.; Myers, A. B. *J. Raman Spectrosc.* **1997**, *28*, 839.

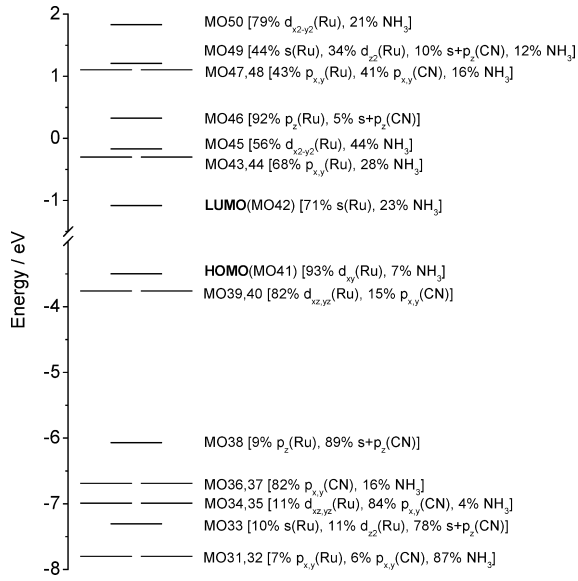

Figure 6. Molecular orbital diagram for model complex *trans*-[$(NH_3)_4Ru(C{\equiv}N)_2$] (**1′**, with C_{2v} symmetry) calculated using HCTH/147 functional and CPCM (solvent = CH_3CN).

and *trans*-$[(NH_3)_4Ru(C{\equiv}N)_2]^+$ (**2′**) were optimized at the DFT level (HCTH/147). In each case, the direction along the N≡C−Ru−C≡N is defined to coincide with the *z* axis of the coordinate system, and the Ru−N bonds in the *x* and *y* directions. The structural data of the optimized structures of **1′** and **2′** (see Supporting Information) are in agreement with related crystal structures. Figures 6 and 7 depict the energy diagrams of several frontier orbitals for both model complexes (calculated with the CPCM to account for the solvent effects of CH_3CN; see the Supporting Information for the detailed molecular orbital plots). For **1′**, the highest occupied molecular orbital (HOMO) is a nonbonding d_{xy}(Ru) orbital. The degenerate HOMO−1 and HOMO−2 are mainly d_{yz}/d_{xz}(Ru) in character (82% $d_{xz,yz}$(Ru), 15% $p_{x,y}$(C≡N)), in which the d_{yz} and d_{xz}(Ru) interact with the π orbital of $^-$C≡N in an antibonding fashion. The d_{yz} and d_{xz}(Ru) are lower in energy than d_{xy}(Ru), consistent with the presence of ruthenium-to-cyanide π-backbonding interaction. For **2′**, the nonbonding d_{xy}(Ru) orbital is singly occupied, revealing that the formation of **2′** corresponds to the removal of one electron from the HOMO (d_{xy} of Ru) of **1′**.

The electronic transitions of **1′** and **2′** in CH_3CN at 298 K have been investigated using TD-DFT method. A comparison of the calculated vertical transition energies of the model complexes and the experimental data for the corresponding complexes is summarized in Table 4. For **1′**, its lowest-energy dipole-allowed electronic transitions at λ_{max} ca. 224 nm (oscillator strength = 0.0804−0.5478) mainly arise from one-electron excitation from the $d_{xz}/d_{yz}(Ru^{II})$ (MO39,40) to π^*(N≡C−Ru−C≡N) orbital (MO47,48; the π system delocalizes along the N≡C−Ru−C≡N moiety), with smaller contributions from $\sigma(^-C{\equiv}N)$ (MO38) to a s + d_{z^2} (sd) hybridized orbital of Ru (MO49) and $\pi(^-C{\equiv}N)$ (MO36,37) to s(Ru) (MO42). Complex **2′** features an intense dipole-allowed electronic transition at λ_{max} ca. 222 nm (oscillator strength = 0.0255−0.0634). Important contributions to these transitions include $d_{xz}/d_{yz}(Ru^{III})$ (MO39β,40β) → π^*(N≡C−Ru−C≡N) (MO44β,45β,48β,49β), $\sigma(^-C{\equiv}N)$ (MO38β) → sd(Ru^{III}) (MO43β), and $\pi(^-C{\equiv}N)$ (MO37α,38α) → sd(Ru^{III}) (MO43α). These calculated intense transitions of **1′** and **2′** match well with their corresponding experimental spectra (λ_{max} = 230 and 228 nm for **1** and **2**, respectively). As **2** also features some moderate intense absorption around 300−400 nm, which appears to be vibronically allowed, we have also examined the transitions with an oscillator strength < 0.005 calculated in this spectral region. The nature of these transitions includes (i) $d_{xz}/d_{yz}(Ru^{III})$ → sd(Ru^{III}), (ii) $\sigma(^-C{\equiv}N)$ → $d_{x^2-y^2}(Ru^{III})$, (iii) NH_3 → $d_{xy}(Ru^{III})$, and (iv) $d_{xz}/d_{yz}(Ru^{III})$ → $d_{x^2-y^2}(Ru^{III})$. Assuming **2′** possesses a C_{2v} symmetry, the irreducible representation of its $\nu_{C\equiv N}$ would transform as $2A_1$, and thus in principle the calculated transitions i−iv should be able to couple with $\nu_{C\equiv N}$.

Discussion

General Remarks. Transition metal ions interact with cyanide ligand through both σ and π interactions; the latter could either be metal-to-cyanide π-backbonding or cyanide-to-metal π-bonding interactions. In this work, we found that increasing the oxidation state from Ru(II) (**1**) to Ru(III) (**2**) leads to an increase in $\nu_{C\equiv N}$ by 70 cm^{-1}, and the $\nu_{C\equiv N}$ for **1** (2031 cm^{-1}) is significantly lower than that in *cis*-$[Ru(dmpe)_2(C{\equiv}N)_2]$ (2102 cm^{-1}, dmpe = bis(dimethylphosphino)ethane),[20] where 16-TMC is a pure σ donor. These findings indicate the presence of π-backbonding in the Ru^{II}−C≡N moiety. However, it is interesting to note that (1) the Ru−C/C−N distances in **1** (2.061(4)/1.130(5) Å) are comparable to those in *cis*-$[Ru(dmpe)_2(C{\equiv}N)_2]$ (Ru−C/C−*N* = 2.045(8)/1.130(9) Å),[20] (2) the Ru−C/C−N distances of the Ru−C≡N moieties in both **1** (2.061(4)/1.130(5) Å) and **2** (2.069(5)/1.140(7) Å) are similar, despite the difference in $\nu_{C\equiv N}$ for **1** and **2** (70 cm^{-1}), and (3) these Ru−C distances are similar to those in the acetylide analogue *trans*-[Ru(16-TMC)(C≡CAr)$_2$] (2.073−2.077 Å),[7a] although $^-$C≡CR is a weaker π acceptor than $^-$C≡N. All of these findings reveal that removal of an electron from Ru(II) does not affect the bonding parameters; thus, the prevailing bonding interaction is σ donation from $^-$C≡N to Ru(II) and Ru(III). Interestingly, the Ru−N distances in $[Ru(bpy)_3]^{2+}$ and $[Ru(bpy)_3]^{3+}$ (bpy = 2,2'-bipyridine) are 2.053(2) and 2.057(3) Å, respectively, which are also insensitive to the oxidation states of the ruthenium ions, as in this work.[21]

The Ru(III/II) couple of **1** is significantly more anodic than that of *trans*-[Ru(16-TMC)(C≡CPh)$_2$] ($E_{1/2}$ = −0.74 V) by 840 mV.[7a] This can be accounted for by the higher electronegativity of $^-$C≡N than $^-$C≡CPh, where the former stabilizes Ru(II) to a greater extent. On the other hand, the Ru(III/II) couple of **1** is more cathodic than that of *trans*-$[Ru(16\text{-}TMC)(C{\equiv}N^tBu)_2]^{2+}$ ($E_{1/2}$ = 0.65 V) by 550 mV.[7c] This is due to the difference in electronic charge (neutral for cyanide complex **1** and dicationic for the isocyanide complex). We envision that **1** or **2** is a good building block

(20) Jones, W. D.; Kosar, W. P. *Organometallics* **1986**, *5*, 1823.
(21) Biner, M.; Bürgi, H.-B.; Ludi, A.; Röhr, C. *J. Am. Chem. Soc.* **1992**, *114*, 5197.

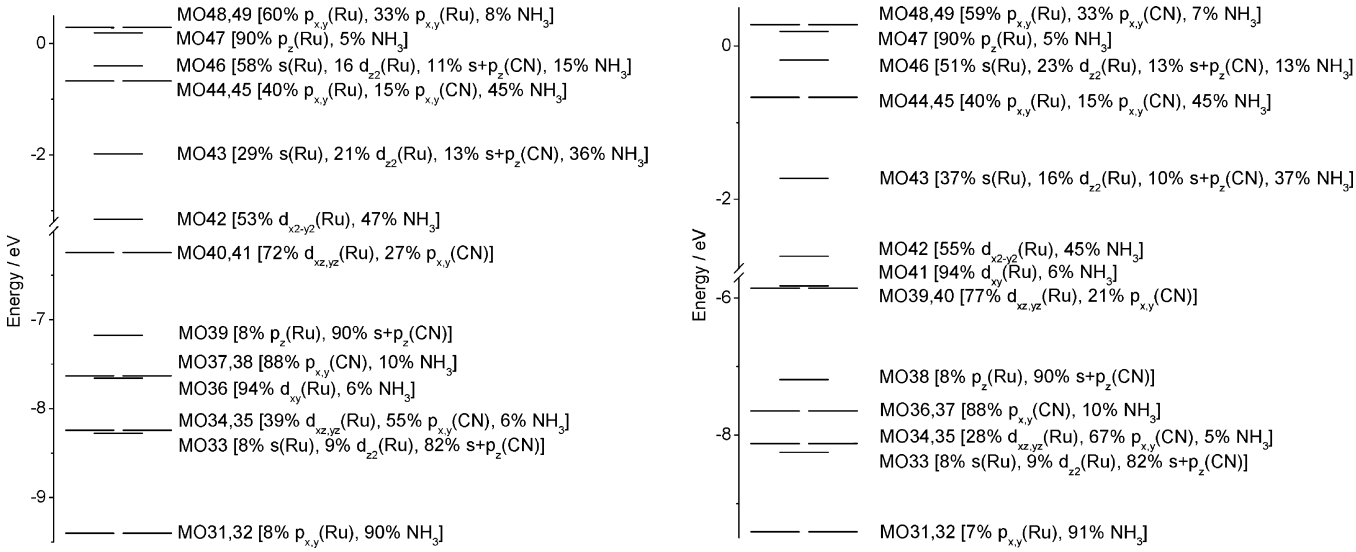

Figure 7. α- (left) and β-spin (right) molecular orbital diagrams for model complex *trans*-$[(NH_3)_4Ru(C{\equiv}N)_2]^+$ (**2′**, without symmetry restriction) calculated using unrestricted HCTH/147 functional and CPCM (solvent = CH_3CN).

Table 4. Comparison of the Vertical Transition Energies for the Model Complexes **1′** and **2′** with Their Corresponding Experimental Data

	TD-DFT calculations		experimental data	
	excitation energy/cm^{-1} (oscillator strength)	transition		λ_{max}/cm^{-1} (ε_{max})
1′	44640 (0.5478)	MO39,40 [82% d$_{xz,yz}$(Ru), 15% p$_{x,y}$(C≡N)] → MO47,48 [43% p$_{x,y}$(Ru), 41% p$_{x,y}$(C≡N)]		
		MO38 [9% p$_z$(Ru), 89% s,p$_z$(C≡N)] → MO49 [44% s(Ru), 34% d$_{z^2}$(Ru), 10% s,p$_z$(C≡N)]	**1**	43480 (11610) 43480 (11610)
	45380 (0.0804)	MO36,37 [82% p$_{x,y}$(C≡N), 16% NH$_3$] → MO42 [71% s(Ru), 23% NH$_3$]		
2′	44920 (0.0634)	MO39β,40β [77% d$_{xz,yz}$(Ru), 21% p$_{x,y}$(C≡N)] → MO44β,45β [40% p$_{x,y}$(Ru), 45% NH$_3$, 15% p$_{x,y}$(C≡N)]	**2**	43860 (br, 17590)
		MO39β,40β [77% d$_{xz,yz}$(Ru), 21% p$_{x,y}$(C≡N)] → MO48β,49β [59% p$_{x,y}$(Ru), 7% NH$_3$, 33% p$_{x,y}$(C≡N)]		
		MO38β [8% p$_z$(Ru), 90% s,p$_z$(C≡N)] → MO43β [37% s(Ru), 37% NH$_3$, 16% d$_{z^2}$(Ru), 10% s,p$_z$(C≡N)]		
	45080 (0.0255)	MO37α,38α [10% NH$_3$, 88% p$_{x,y}$(C≡N)] → MO43α [29% s(Ru), 21% d$_{z^2}$(Ru), 36% NH$_3$, 13% s,p$_z$(C≡N)]		43860 (br, 17590)
	27340 (<0.0001)	MO40α,41α [72% d$_{xz,yz}$(Ru), 27% p$_{x,y}$(C≡N)]→ MO42α [53% d$_{x^2-y^2}$(Ru), 47% NH$_3$]		26600−31750 (470−760)
		MO39β,40β [77% d$_{xz,yz}$(Ru), 21% p$_{x,y}$(C≡N)] → MO42β [55% d$_{x^2-y^2}$(Ru), 45% NH$_3$]		
	28400 (0.0016)	MO31β,32β [7% p$_{x,y}$(Ru), 91% NH$_3$] → MO41β [94% d$_{xy}$(Ru), 6% NH$_3$]		26600−31750 (470−760)
	32390 (<0.0001)	MO39α [8% p$_z$(Ru), 90% s,p$_z$(C≡N)] → MO42α [53% d$_{x^2-y^2}$(Ru), 47% NH$_3$]		26600−31750 (470−760)
	32450 (<0.0001)	MO39β,40β [77% d$_{xz,yz}$(Ru), 21% p$_{x,y}$(C≡N)] → MO43β [37% s(Ru), 37% NH$_3$, 16% d$_{z^2}$(Ru), 10% s,p$_z$(C≡N)]		26600−31750 (470−760)

for molecular electronics because **1** and **2** are interconvertible electrochemically and they do not suffer large structural change before and after the conversion (as suggested by the X-ray structural data).

Absorption Spectroscopy. Complex **1** exhibits an intense high-energy absorption band at λ_{max} = 230 nm with an ε_{max} value in excess of 10^3 dm^3 mol^{-1} cm^{-1}, indicating a dipole-allowed electronic transition. As KCN is optically transparent in the spectral window (200−800 nm), this absorption band should be originated from the Ru−C≡N moiety, and a tentative assignment would be a $d_\pi(Ru^{II}) \rightarrow \pi^*(C{\equiv}N)$ metal-to-ligand charge-transfer (MLCT) transition. TD-DFT calculation on model complex **1′** suggests a similar assignment: the calculated transition at λ_{max} of ca. 224 nm mainly arises from a $d_{xz}/d_{yz}(Ru^{II}) \rightarrow \pi^*(N{\equiv}C-Ru-C{\equiv}N)$ charge transfer transition, accompanied by some $\pi(^-C{\equiv}N) \rightarrow$ s(Ru) and $\sigma(^-C{\equiv}N) \rightarrow$ sd (Ru) characters. The $d_{xz}/d_{yz}(Ru^{II}) \rightarrow \pi^*(N{\equiv}C-Ru-C{\equiv}N)$ transition energy of **1** is red-shifted from the $^1A_g \rightarrow {}^1T_{1u}$ $d_\pi(Ru^{II}) \rightarrow \pi^*(C{\equiv}N)$ MLCT transition (192 and 206 nm) of $[Ru(C{\equiv}N)_6]^{4-}$.[6a] This is consistent with the stronger ligand-field strength of $^-C{\equiv}N$ than that of amine-type ligands like 16-TMC in this work. Also, the $d_{xz}/d_{yz}(Ru^{II}) \rightarrow \pi^*(N{\equiv}C-Ru-C{\equiv}N)$ charge-transfer assignment is consistent with the result obtained in the resonance Raman experiment that the absorption band at λ_{max} = 230 nm of **1** is strongly coupled to the nominal $\nu_{C{\equiv}N}$ stretch mode (see the Resonance Raman Spectroscopy section). Weak absorptions of **1** at λ_{max} = 316, 389, and 490 (ε_{max} < 100 dm^3 mol^{-1} cm^{-1}) are dipole-forbidden and are assigned to d−d transitions. The lowest-energy d−d transition of **1** at 490 nm is lower in energy than the $^1A_g \rightarrow {}^1T_g$ d−d

transition of $[Ru(C\equiv N)_6]^{4-}$ ($\lambda_{max} = 323$ nm),[6a] consistent with $^{-}C\equiv N$ having a stronger ligand field strength than the amine ligand.

Although complex **2** also features strong high-energy absorptions at λ ca. 230 nm (a peak maximum at $\lambda_{max} = 228$ nm ($\varepsilon_{max} > 10^3$ dm^3 mol^{-1} cm^{-1}) is recorded), comparison through overlaying the absorption spectra of **1** and **2** (Figure 3) clearly shows some differences: **2** contains broader absorption at $\lambda < 230$ nm. Unfortunately, investigation into the higher-energy region is hampered by solvent absorption bands and instrumental limitation. TD-DFT calculation on **2′** suggests that the intense absorption at 228 nm is dominated by $d_{xz}/d_{yz}(Ru^{III}) \rightarrow \pi^*(N\equiv C-Ru-C\equiv N)$ and $\sigma(^{-}C\equiv N) \rightarrow sd(Ru^{III})$ transitions, accompanied by some $\pi(^{-}C\equiv N) \rightarrow sd(Ru^{III})$ charge transfer character. The resemblance in the high-energy absorption between **1** ($\lambda_{max} = 230$ nm) and **2** (228 nm) is not surprising because both complexes have similar transitions of $d_{xz}/d_{yz}(Ru) \rightarrow \pi^*(N\equiv C-Ru-C\equiv N)$ at this spectral region, and the oxidation of **1**, corresponding to the removal of an electron from a nonbonding $d_{xy}(Ru)$ orbital, should have little effect on the energy for the $d_{xz}/d_{yz}(Ru) \rightarrow \pi^*(N\equiv C-Ru-C\equiv N)$ transition. It is also interesting to note that the $d_\pi(Fe) \rightarrow \pi^*(^{-}C\equiv N)$ MLCT transitions of $[Fe(C\equiv N)_6]^{4-}$ ($\lambda_{max} = 200$, 218 nm) and $[Fe(C\equiv N)_6]^{3-}$ ($\lambda_{max} = 200$, 227 nm) are virtually the same energy.[6b]

The weak bands of **2** with peak maxima at 315, 333, 354, and 376 nm ($\varepsilon_{max} = (3-8) \times 10^2$ dm^3 mol^{-1} cm^{-1}) could be due to vibronic coupling with a C≡N stretch since the energy spacings between adjacent peak maxima are 1720, 1780, and 1650 cm^{-1}, all of which match the $\nu_{C\equiv N}$ in the electronic excited state. However, the possibility of the vibrational satellite structure to be originated from Franck−Condon progression should not be excluded. In any case, TD-DFT calculation suggests that the possible electronic transitions in this spectral region include (i) $d_{xz}/d_{yz}(Ru^{III}) \rightarrow sd(Ru^{III})$, (ii) $\sigma(^{-}C\equiv N) \rightarrow d_{x^2-y^2}(Ru^{III})$, (iii) $NH_3 \rightarrow d_{xy}(Ru^{III})$, and (iv) $d_{xz}/d_{yz}(Ru^{III}) \rightarrow d_{x^2-y^2}(Ru^{III})$ transitions, and they are all able to couple with $\nu_{C\equiv N}$ as the $\nu_{C\equiv N}$ of **2′** transforms as $2A_1$ under a C_{2v} symmetry. We suggest that the calculated $\sigma(^{-}C\equiv N) \rightarrow d_{x^2-y^2}(Ru^{III})$ ligand-to-metal charge-transfer (LMCT) transition could be an important origin for these vibronic transitions, as it involves the $\sigma(^{-}C\equiv N)$ orbital. Interestingly, Gray and Alexander assigned the lowest-energy weak absorption of $[^nBu_4N]_3[Fe(C\equiv N)_6]$ at $\lambda_{max} = 426$ nm to $\sigma(^{-}C\equiv N) \rightarrow d_\pi(Fe^{III})$ LMCT transition on the basis of molecular orbital calculations.[6b]

Resonance Raman Spectroscopy. By simulating the 230 nm absorption band and the resonance Raman intensities of **1**, it was estimated that the nominal $\nu_{C\equiv N}$ stretch mode accounts for approximately 66% of the total vibrational reorganization energy. This indicates that the absorption band is strongly coupled to the cyanide ligand. If we assume that the nominal $\nu_{C\equiv N}$ stretch mode can be approximated by a pure C≡N stretch, the change in bond length along the C−N bond in the initially formed excited state can be calculated from

$$q = (\mu\omega/\hbar)^{1/2}(\Delta x) \quad (1)$$

where q is the dimensionless normal coordinate, μ is the reduced mass of the C≡N bond, ω is the ground-state vibrational frequency, and Δx is the change of bond length. Using the parameters for *trans*-[Ru(16-TMC)$(C\equiv N)_2$] given in Table 3, a change in bond length of about 0.054 Å in the excited state relative to the ground state was estimated using eq 1. This change in C−N bond length is consistent with a nominal bond order change from 3 to 2.5, which is expected for a $d_\pi(Ru^{II}) \rightarrow \pi^*(N\equiv C-Ru-C\equiv N)$ charge transfer transition. Interestingly, the vibrational reorganizational energies for the electronic transition of **1** (300 cm^{-1} total with 66% in the C≡N stretch mode) are similar to those for the MLCT transition in *trans*-[Ru(16-TMC)$(C\equiv CPh)_2$] (643 cm^{-1} total with 60% in the C≡C and C=C stretch mode)[7e] in both magnitude and percentage in the unsaturated ligand vibrational mode.

Conclusion

trans-[Ru(16-TMC)$(C\equiv N)_2$] (**1**) and *trans*-[Ru(16-TMC)-$(C\equiv N)_2](PF_6)$ (**2**·PF_6) have been prepared. The structural difference between these two complexes is minimal. The lower $\nu_{C\equiv N}$ for **1** compared to **2** suggests the presence of a Ru^{II}-to-cyanide π-backbonding interaction in **1**, although this could not be the major bonding interaction between $^{-}C\equiv N$ and Ru(II)/Ru(III) ions. The $d_\pi(Ru^{II}) \rightarrow \pi^*(^{-}C\equiv N)$ MLCT transition of **1** at $\lambda_{max} = 230$ nm has been probed by resonance Raman spectroscopy, revealing that the nominal $\nu_{C\equiv N}$ stretch mode accounts for ca. 66% of the total vibrational reorganization energy. Vibronic features are observed in the $\sigma(^{-}C\equiv N) \rightarrow d(Ru^{III})$ LMCT transition for **2** at $\lambda_{max} = 315-441$ nm.

Acknowledgment. This work was supported by City University of Hong Kong [Project No. 7200084 (C.-Y.W.)] and Hong Kong Research Grants Council [Project No. HKU 7012/05, HKU 7011/07 (C.-M.C.)]. We also thank Professor Harry B. Gray for helpful discussion.

Supporting Information Available: Optimized geometries for **1′** and **2′**; energies, compositions, and surface plot of the frontier molecular orbitals for **1′** and **2′**; crystallographic information files (CIF) for **1** and **2**. This material is available free of charge via the Internet at http://pubs.acs.org.

IC800743A